Proceedings of IDETC/CIE 2009
ASME 2009 International Design Engineering Technical Conferences &
Computers and Information in Engineering Conference
August 30 - September 2, 2009, San Diego, California, USA

DETC2009-86883

DYNAMICS OF NON-IDEAL TOPOLOGY TRANSITIONS IN MULTIBODY MECHANICAL SYSTEMS

Josep M. Font-Llagunes*
Department of Mechanical Engineering
Universitat Politècnica de Catalunya
Barcelona 08028, Catalunya, Spain
E-mail: josep.m.font@upc.edu

József Kövecses
Centre for Intelligent Machines
Department of Mechanical Engineering
McGill University
Montréal H3A 2K6, Québec, Canada
E-mail: jozsef.kovecses@mcgill.ca

ABSTRACT

Mechanical systems with time-varying topology appear frequently in various applications. In this paper, topology changes that can be modeled by means of bilateral impulsive constraints are analyzed. We present a concept to project kinematic and kinetic quantities to two mutually orthogonal subspaces of the tangent space of the mechanical system. This can be used to obtain decoupled formulations of the kinetic energy and the dynamic equations at topology transition. It will be shown that the configuration of the multibody system at topology change significantly influences the projection of non-ideal forces to both subspaces. Experimental analysis, using a dual-pantograph robotic prototype interacting with a stiff environment, is presented to illustrate the material.

NOMENCLATURE

$\mathbf{A}$ Jacobian associated with constrained motion.
$\mathbf{B}$ Jacobian associated with tangential directions of contact.
$\mathbf{M}$ Mass matrix of the system.
$\mathbf{P}_a$ Projector associated with the space of admissible motion.
$\mathbf{P}_c$ Projector associated with the space of constrained motion.
$\mathbf{q}$ Generalized coordinates of the system.
$\mathbf{v}$ Generalized velocities of the system.
$\mathbf{v}_a$ Generalized velocities of the space of admissible motion.
$\mathbf{v}_c$ Generalized velocities of the space of constrained motion.
$\bar{\mathbf{f}}_A$ Generalized applied impulses.
$\bar{\mathbf{f}}_N$ Generalized non-ideal impulses.
$\bar{\mathbf{f}}_R$ Generalized constraint impulses.
T Kinetic energy of the system.
T_a Kinetic energy of the space of admissible motion.
T_c Kinetic energy of the space of constrained motion.

INTRODUCTION

Variable topology mechanical systems are present in various fields of applications such as robotics, biomechanics and mechanism science. The dynamic analysis of such systems depends on the time-varying nature of the connections between the elements of the system and the environment. This complicates the analysis because in most cases a different dynamic model must be developed for each constraint condition. Typical situations that occur in variable topology systems are the following:

(1) The number of degrees of freedom of the system decreases via the development of certain connections. An example for this can be the grasping/capturing of a moving payload, which may also represent the interaction of two robotic mechanisms, or a human and a payload. The effect of mass capture on flexible multibody systems was studied in [1] and [2]. This group of problems includes two possibilities depending on whether the developed connections exist for a finite period of time or they represent an instantaneous situation.

*Address all correspondence to this author.

(2) The constraint configuration is changing: some constraints are added and some become passive. But, the effective number of degrees of freedom may stay the same. An example for this situation can be found in the analysis of (active/passive) dynamic walking machines [3]. In those systems, the heel strike event represents a sudden change of topology where some constraints are imposed on the foot that makes contact, and other are released from the foot that leaves the ground [4, 5].

Discontinuous constraints have been a known concept in analytical mechanics [6–8]. As discussed earlier, two particular cases of such discontinuous constraint configurations can be the sudden removal and the sudden addition of constraints. The sudden removal of constraints alone does not instantaneously change the energy and momentum distribution of the system unless other impulsive forces (applied or constraint forces) are present.

The sudden addition of constraints does cause instantaneous changes. Therefore, this is the truly critical event during the motion of variable topology systems. Such events can be characterized using "inert constraints" which are a class of impulsive constraints [6, 8].

This paper focuses on this event of sudden addition of constraints. We consider the general case of non-ideal development of constraints, i.e., we consider that impulsive forces can also be present along the tangential direction of the contact, e.g., due to friction or finite tangential stiffness of materials. It is not the aim of the work to model these impulses, but to understand their effect on the impulsive dynamics of topology transition.

The dynamic analysis conducted in the paper is based on an analytical approach that allows a complete decoupling of the dynamic equations and the kinetic energy to two subspaces of the tangent space of the system, i.e., the spaces of constrained and admissible motions [9]. Based on this approach, it will be shown that the effects of non-ideal impulsive forces on the decoupled dynamic equations vary depending on the system configuration at topology transition. To illustrate this, detailed experimental analysis using a dual-pantograph robotic device is conducted.

DYNAMICS MODELING

Let us consider that the configuration of the system can be described by n generalized coordinates that are represented by $n \times 1$ dimensional array $\mathbf{q}$. The time derivatives of these generalized coordinates $\dot{\mathbf{q}}$ give a possible set of generalized velocities of the system. We will use a more general description for the velocities employing components collected in $\mathbf{v}$, which can be interpreted as general linear combinations of the time derivatives of the generalized coordinates as $\mathbf{v} = \mathbf{N}\dot{\mathbf{q}}$ and $\dot{\mathbf{q}} = \mathbf{N}^{-1}\mathbf{v}$, where $\mathbf{N}$ is an $n \times n$ transformation matrix that can depend on the generalized coordinates and time. We will consider that this parameterization represents a minimum set of generalized coordinates and velocities with respect to the continuous constraints imposed on the system.

In this paper, we will primarily consider systems where the kinetic energy can be expressed as a quadratic function of the generalized velocities

$$T = \frac{1}{2}\mathbf{v}^T\mathbf{M}\mathbf{v} \tag{1}$$

where $\mathbf{M}(\mathbf{q})$ is the mass matrix of the system. The dynamic equations for parameterization ($\mathbf{v}$, $\mathbf{q}$) can generally be written as

$$\mathbf{M}\dot{\mathbf{v}} + \mathbf{c}(\mathbf{v},\mathbf{q}) = \mathbf{f}_A + \mathbf{f}_R + \mathbf{f}_N \tag{2}$$

where $\mathbf{c}(\mathbf{v},\mathbf{q})$ represents the Coriolis and centrifugal effects, $\mathbf{f}_A$ and $\mathbf{f}_R$ are the generalized applied and constraint forces, and $\mathbf{f}_N$ represents generalized non-ideal forces that may arise due to the non-ideal realization of constraints. The explicit expressions of the generalized constraint and non-ideal forces $\mathbf{f}_R$ and $\mathbf{f}_N$ will be associated with discontinuous impulsive constraints only.

Let us consider that t_i represents the time when certain constraints are suddenly established and, as a result, the topology of the system changes. This sudden addition/imposition of physical connections can be modeled by means of inert constraints [6, 8].

The event of topology transition takes place in the $[t_i^-,\, t_i^+]$ interval, where t_i^- and t_i^+ represent the so-called pre- and post-event instants. The duration of this interval can usually be considered very short on the characteristic time scale of the finite (continuous) motion of the system. Therefore, the configuration of the system is assumed to be constant in $[t_i^-,\, t_i^+]$, and the event of topology change is analyzed as an impulsive motion event. Inert constraints can normally be written as

$$\mathbf{A}\mathbf{v}^+ = \mathbf{0} \tag{3}$$

where $\mathbf{v}^+$ stands for $\mathbf{v}$ at t_i^+, and $\mathbf{A}$ is the $m \times n$ dimensional constraint Jacobian. Note that Eq. (3) represents the required topology of the mechanical system at t_i^+ at the velocity level.

Two typical situations may arise depending on whether the new constraints persist for a finite period of time or they represent an instantaneous situation. One example for the first situation appears in bipedal locomotion when the swing leg makes contact with the ground at heel strike. The dynamics of heel strike in a bipedal compass walker with upper body was analyzed by the authors in [10].

For the second situation, an example can be the general consideration of low velocity impact between two bodies when the duration of the impact "looks" instantaneous on the characteristic time scale determined by the finite motion of the system. Such impact can be divided to two phases (namely, compression

and restitution phases) and the system configuration is usually assumed constant during the whole event. The compression phase can be modeled with constraints of the form of Eq. (3), where $\mathbf{v}^+$ denotes the generalized velocities at the end of compression when the relative normal velocity of the contact points is zero. This case will be experimentally analyzed further in this paper.

Projection Operators and Decomposition

The tangent space of the dynamic system can be seen as an n dimensional linear space interpreted for each configuration [11, 12]. Since the configuration of the system is assumed to be unchanged in the $[t_i^-,\, t_i^+]$ interval, a single interpretation of this linear space may be used for both the pre- and post-event instants. The inert constraints and their Jacobian $\mathbf{A}$ can be employed to decompose this tangent space to the space of constrained motion (SCM) and space of admissible motion (SAM) [9].

The above two subspaces can be defined so that they are orthogonal to each other with respect to the mass metric of the tangent space [9, 13]. In this case, any impulsive event characterized by ideal inert constraints of the form of Eq. (3) will influence quantities in the space of constrained motion leaving the space of admissible motion unaffected. However, non-ideal effects can couple the two subspaces and develop an influence on the admissible motion dynamics too. The decomposition to the two subspaces can be accomplished using two projection operators $\mathbf{P}_c$ (for the SCM) and $\mathbf{P}_a$ (for the SAM) [9, 13]. They take the following expressions

$$\mathbf{P}_c = \mathbf{M}^{-1}\mathbf{A}^T\left(\mathbf{A}\mathbf{M}^{-1}\mathbf{A}^T\right)^{-1}\mathbf{A} \tag{4}$$

$$\mathbf{P}_a = \mathbf{I} - \mathbf{P}_c = \mathbf{I} - \mathbf{M}^{-1}\mathbf{A}^T\left(\mathbf{A}\mathbf{M}^{-1}\mathbf{A}^T\right)^{-1}\mathbf{A} \tag{5}$$

where $\mathbf{I}$ is the $n \times n$ dimensional identity matrix. It can be seen that the projectors above satisfy that $\mathbf{P}_a^T\mathbf{M}\mathbf{P}_c = \mathbf{0}$, where $\mathbf{0}$ denotes the $n \times n$ zero matrix. This shows the orthogonality of $\mathbf{P}_c$ and $\mathbf{P}_a$ with respect to the mass metric $\mathbf{M}$.

Using the above operators, the generalized velocities of the system can be decomposed as

$$\mathbf{v} = \mathbf{v}_c + \mathbf{v}_a = \mathbf{P}_c\mathbf{v} + \mathbf{P}_a\mathbf{v} \tag{6}$$

where $\mathbf{v}_c = \mathbf{P}_c\mathbf{v}$ and $\mathbf{v}_a = \mathbf{P}_a\mathbf{v}$ represent the two components associated with the SCM and SAM, respectively. Based on Eq. (6), it can be seen that the kinetic energy can also be decomposed as

$$T = T_c + T_a = \frac{1}{2}\mathbf{v}_c^T\mathbf{M}\mathbf{v}_c + \frac{1}{2}\mathbf{v}_a^T\mathbf{M}\mathbf{v}_a \tag{7}$$

which represents a complete decoupling of T [9, 13]. To obtain Eq. (7) it was used that $\mathbf{v}_a^T\mathbf{M}\mathbf{v}_c = 0$, which is a direct consequence of the orthogonality of the projectors with respect to $\mathbf{M}$. Any vector of generalized forces or generalized impulses can also be decomposed using the transpose of $\mathbf{P}_c$ and $\mathbf{P}_a$ as

$$\mathbf{f} = \mathbf{f}_c + \mathbf{f}_a = \mathbf{P}_c^T\mathbf{f} + \mathbf{P}_a^T\mathbf{f} \quad \text{and} \quad \bar{\mathbf{f}} = \bar{\mathbf{f}}_c + \bar{\mathbf{f}}_a = \mathbf{P}_c^T\bar{\mathbf{f}} + \mathbf{P}_a^T\bar{\mathbf{f}} \tag{8}$$

where $\bar{\mathbf{f}}$ represents the impulse of $\mathbf{f}$. It is also possible to show that $\mathbf{f}_a^T\mathbf{M}^{-1}\mathbf{f}_c = 0$ and $\bar{\mathbf{f}}_a^T\mathbf{M}^{-1}\bar{\mathbf{f}}_c = 0$ hold for the general case.

CHARACTERIZATION OF TOPOLOGY TRANSITIONS WITH NON-IDEAL CONSTRAINT REALIZATION

The dynamics of the instantaneous imposition of constraints can be characterized by impulse-momentum level dynamic equations. Based on Eqs. (1) and (2), these can be obtained in general form as [8, 14]

$$\left[\frac{\partial T}{\partial \mathbf{v}}\right]_-^+ = \mathbf{M}\left(\mathbf{v}^+ - \mathbf{v}^-\right) = \bar{\mathbf{f}}_A + \bar{\mathbf{f}}_R + \bar{\mathbf{f}}_N \tag{9}$$

where "$-$" and "$+$" denote the pre- and post-event instants, $\bar{\mathbf{f}}_A$, $\bar{\mathbf{f}}_R$ and $\bar{\mathbf{f}}_N$ are the impulses of the generalized applied, constraint, and non-ideal forces, respectively. If the applied forces are non-impulsive, then $\bar{\mathbf{f}}_A = \mathbf{0}$. This is the case we primarily consider to gain insight into the effect of inert constraints representing the topology change. The generalized constraint impulses responsible for the topology change can be written as

$$\bar{\mathbf{f}}_R = \mathbf{A}^T\bar{\lambda} \tag{10}$$

where $\bar{\lambda}$ represents the impulse of the normal contact forces developed during this event and $\mathbf{A}$ is the Jacobian in Eq. (3). The impulses of the generalized non-ideal forces can usually be expressed with force laws such as $\bar{\mathbf{f}}_N = \bar{\mathbf{f}}_N(\bar{\lambda}, \mathbf{v}, \mathbf{q})$. If we name $\mathbf{B}$ the Jacobian associated with tangential directions of the contact (i.e., $\mathbf{B}\mathbf{v}$ are velocity components of the contact point along directions where motion is not constrained) then the generalized non-ideal impulses can be expressed as

$$\bar{\mathbf{f}}_N = \mathbf{B}^T\bar{\beta} \tag{11}$$

where $\bar{\beta}$ represents the impulse of the non-ideal forces developed along the tangential directions.

Based on the decompositions introduced in the previous section, the impulsive dynamic equations provided in Eq. (9) can be decoupled by multiplying both sides of the equation with $\mathbf{P}_c^T$ and

$\mathbf{P}_a^T$. The dynamic equations associated with the SCM and the SAM can be respectively expressed as

$$\left[\frac{\partial T_c}{\partial \mathbf{v}_c}\right]_-^+ = \mathbf{M}\left(\mathbf{v}_c^+ - \mathbf{v}_c^-\right) = \mathbf{A}^T\bar{\lambda} + \mathbf{P}_c^T\mathbf{B}^T\bar{\beta} \tag{12}$$

$$\left[\frac{\partial T_a}{\partial \mathbf{v}_a}\right]_-^+ = \mathbf{M}\left(\mathbf{v}_a^+ - \mathbf{v}_a^-\right) = \mathbf{P}_a^T\mathbf{B}^T\bar{\beta} \tag{13}$$

Note that to obtain the last equations it was used that $\mathbf{P}_c^T\mathbf{A}^T = \mathbf{A}^T$ and $\mathbf{P}_a^T\mathbf{A}^T = \mathbf{0}$, this comes directly from the definition of projection operators in Eqs. (4) and (5). Eq. (12) can also be rewritten as

$$\left[\frac{\partial T_c}{\partial \mathbf{v}_c}\right]_-^+ = \mathbf{M}\left(\mathbf{v}_c^+ - \mathbf{v}_c^-\right) = \mathbf{A}^T(\bar{\lambda} + \bar{\Lambda}) \tag{14}$$

where $\mathbf{P}_c^T\mathbf{f}_N^T = \mathbf{A}^T\bar{\Lambda}$ [9]. The decoupled equations provide useful information to analyze the dynamics of topology transitions. First of all, it can be seen that constraint impulses $\bar{\mathbf{f}}_R$ are fully projected to the SCM and, therefore, only impulses due to non-ideal phenomena are present in the equation associated with the SAM. However, non-ideal impulses may have a projection to both the SCM and SAM. Also, based on Eqs. (14), (3) and (6), it can be shown that $\mathbf{v}_c^+ = \mathbf{0}$. Therefore, using Eq. (14) we obtain that

$$-\mathbf{M}\mathbf{v}_c^- = \mathbf{A}^T(\bar{\lambda} + \bar{\Lambda}) \tag{15}$$

Regarding the energetics of the transition, it can be concluded that no matter how much kinetic energy is contained in the SCM at the pre-event time, this will be completely "lost" during topology change since $\mathbf{v}_c^+ = 0$ and therefore $T_c^+ = 0$. According to Eq. (13), the kinetic energy of the SAM can change during topology transition due to non-ideal impulses. In the case of ideal transition, i.e., $\bar{\mathbf{f}}_N = \mathbf{0}$, then $\mathbf{v}^+ = \mathbf{v}_a^+ = \mathbf{v}_a^-$ and thus $T^+ = T_a^+ = T_a^-$. In such a case, the total energy loss due to the sudden addition of constraints would be T_c^-. However, the presence of non-ideal impulsive forces can make the kinetic energy T_a vary during the transition interval $[t_i^-, t_i^+]$.

Finally, based on Eqs. (6), (7) and (15), and using that $\mathbf{v}_a^T\mathbf{M}\mathbf{v}_c = 0$, it is possible to write that

$$-(\mathbf{v}^-)^T\mathbf{M}\mathbf{v}_c^- = -2T_c^- = (\mathbf{v}^-)^T\mathbf{A}^T(\bar{\lambda} + \bar{\Lambda}) \tag{16}$$

which establishes an explicit relationship between the magnitude of the impulses generated at topology change and the pre-event kinetic energy content in the SCM, T_c^-. As said before, this is completely lost once the constraint is established and Eq. (3) satisfied.

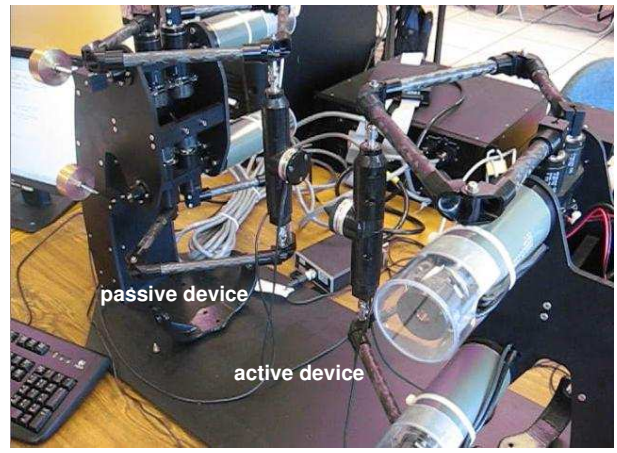

Figure 1. Experimental set-up based on two dual-pantograph devices

EXPERIMENTAL SET-UP

An experimental testbed based on two dual-pantograph devices has been used to investigate the concepts introduced earlier in this paper. This is shown in Fig. 1. Each device is equipped with high-resolution force/torque sensors at the tip and optical encoders at the motor joints. For our present study, one of these devices (passive device) emulates a stiff environment with a flat surface and the other (active device) comes to a contact interaction with the passive one at one single contact point. An interface with a conical shape is mounted onto the end effector of the active device to ensure point contact with the flat end plate of the passive system. The compression phase associated with this interaction represents a topology transition that can be modeled with inert constraints.

Although a single device can move the end effector with the 6-DOF of general 3D motion, the trajectories performed have been programmed so that the motion of the system can be considered planar. The planes of the two pantographs are parallel so they can be considered with one single "composite" pantograph model, Fig. 2. As it can be seen in this figure, angles q_i denote the absolute orientation of the ith link ($i = 1,2,3,4$) of the pantograph.

Regarding the parameters of the system, l_i and a_i represent the length and the position of the center of mass of the ith link, m_i and I_i denote its mass and moment of inertia about its center of mass, and m_{EE} denotes the mass of the end effector. Parameter l_5 indicates the distance between the two motors. The value for these parameters can be found in Table 1.

For planar motion, the system can be considered as a 2-DOF mechanism and the actuated joint coordinates $\mathbf{q} = [q_1\ q_3]^T$ and their time derivatives $\mathbf{v} = \dot{\mathbf{q}}$ may be used as independent gener-

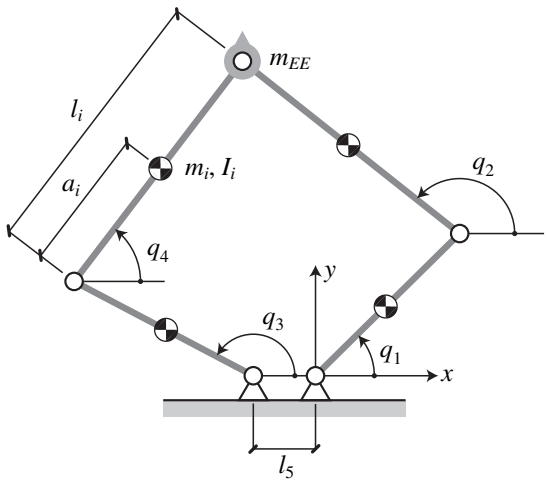

Figure 2. Planar dynamic model of the pantograph

alized coordinates and velocities, respectively. Using this representation, the mass matrix **M** has been determined.

Since in the experiments the flat end plate of the passive device has a normal parallel to the y axis, the topology transition can be represented with one inert constraint that describes the sudden imposition of the physical contact constraint on the end point velocity of the active device along the y direction. Therefore, we can express this constraint as $\dot{y}_{EE}^{+} = \mathbf{A}\mathbf{v}^{+} = 0$. Jacobian **B** is associated with the motion of the end point along the "unconstrained" x direction. From Jacobians **A** and **B**, the velocity

Table 1. Dynamic parameters of the pantograph

Parameter	Value	Description
l_1, l_3	0.1449 m	Length of links 1,3
l_2, l_4	0.1984 m	Length of links 2,4
a_1, a_3	0.0519 m	Position of COM of links 1,3
a_2, a_4	0.1081 m	Position of COM of links 2,4
l_5	0.0445 m	Dist. between actuated joints
m_1, m_3	0.1202 kg	Mass of links 1,3
m_2, m_4	0.1084 kg	Mass of links 2,4
m_{EE}	0.3144 kg	Mass of end effector
I_1, I_3	0.0004 kgm^2	Moment of inertia of links 1,3
I_2, I_4	0.0007 kgm^2	Moment of inertia of links 2,4

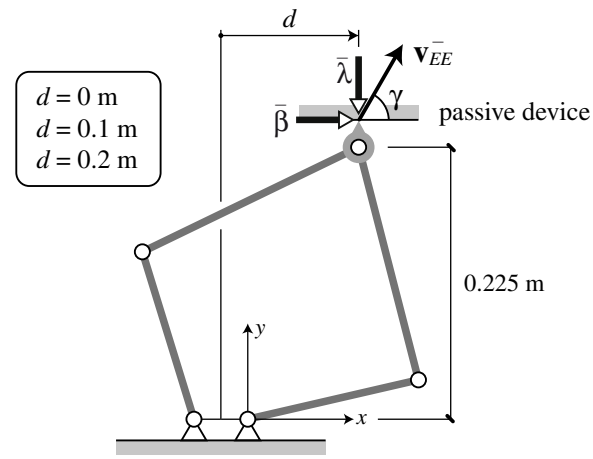

Figure 3. Experimental conditions

$\mathbf{v}_{EE}$ of the end point in inertial frame coordinates is

$$\mathbf{v}_{EE} = \begin{bmatrix} \dot{x}_{EE} \\ \dot{y}_{EE} \end{bmatrix} = \begin{bmatrix} \mathbf{B} \\ \mathbf{A} \end{bmatrix} \mathbf{v} \tag{17}$$

We have developed experiments to test the influence of the system configuration on the dynamics of the topology transition. We have considered three different configurations obtained by modifying parameter d, shown in Fig. 3, which takes the following three values: $d = 0$ m, $d = 0.1$ m, and $d = 0.2$ m. For each contact configuration, the velocities $\mathbf{v}$ at t_i^- have been defined such that the velocity of the end effector forms an angle γ with the x direction (see Fig. 3) and T_c^- is constant for all the experimental conditions. Two angles have been considered for each configuration: $\gamma = 90°$ (velocity perpendicular to the stiff wall) and $\gamma = 60°$.

A normal impulse $\bar{\lambda}$ is generated due to the imposition of the constraint in the normal direction. Also, a non-ideal impulse $\bar{\beta}$ appears along the tangential direction due to friction and tangential stiffness of the contact. These impulses are represented in Fig. 3 and they have been measured for each experimental condition integrating the force measurements over interval $[t_i^-, t_i^+]$. The numerical integration has been done via the trapezoidal method using the sample time of the data acquisition system, i.e., $\Delta t = 0.001$ s.

An interesting parameter that will be evaluated in the following is the ratio ξ between the pre-event kinetic energy associated with the SCM (which is lost) and the total pre-event kinetic energy of the system. This can be expressed as

$$\xi = \frac{T_c^-}{T^-} = \frac{(\mathbf{v}^-)^T \mathbf{P}_c^T \mathbf{M} \mathbf{P}_c \mathbf{v}^-}{(\mathbf{v}^-)^T \mathbf{M} \mathbf{v}^-} \tag{18}$$

and gives information on what part of the initial kinetic energy

is required to develop the constraint forces. This parameter has two extreme values (0 and 1) which are associated with different directions of the tangent space of the multibody system. These directions can be obtained via the formulation of an eigenvalue problem as it is explained in [15].

RESULTS AND DISCUSSION

The following results have been obtained using the robotic system described above. Six different experimental conditions have been tested: $d = 0$ m and $\gamma = 90°$, $d = 0$ m and $\gamma = 60°$, $d = 0.1$ m and $\gamma = 90°$, $d = 0.1$ m and $\gamma = 60°$, $d = 0.2$ m and $\gamma = 90°$, and $d = 0.2$ m and $\gamma = 60°$. These are named cases 1 to 6, respectively. Each experiment has been repeated several times and the results averaged to obtain better estimations of them. Fig. 4 shows the evolution of the kinetic energy decomposition (T_c and T_a) for one individual experiment corresponding to each case. The white spots in the plots indicate the considered values of T_c and T_a at t_i^- (just before contact) and t_i^+ (end of compression). Note that the obtained value of T_c at t_i^+ is zero in all cases, this represents the instant when the inert constraint is established, $\dot{y}_{EE}^+ = 0$. In the plots that correspond to cases 1 and 3, it can be seen that T_a is almost zero during all the experiment.

Table 2 shows the results for the pre- and post-event kinetic energy redistribution for each case. It can be seen that $T_c^+ \approx 0$ (as expected) and that T_a varies in cases 2, 4, and 6 due to the appearance of non-ideal forces during contact (such cases are the ones with $\gamma = 60°$). In cases 1, 3, and 5; non-ideal effects are lower because $\dot{x}_{EE}^- = 0$ ($\gamma = 90°$) and T_a experiences less change. As it will be shown the tangential impulse $\bar{\beta}$ is lower when $\gamma = 90°$. Parameter ξ gives the proportion of the pre-impact kinetic energy that is projected to the SCM, Eq. (18). As shown before, this part of the kinetic energy is lost when constraints are imposed. It can be seen that ξ depends both on configuration $\mathbf{q}$ and velocities $\mathbf{v}^-$.

Table 3 shows the measured impulses $\bar{\lambda}$ and $\bar{\beta}$. It can be seen that for cases 2, 4, and 6 the impulse $\bar{\beta}$ along the tangential direction is larger than in the other cases. The negative sign of the impulse is due to fact that $\dot{x}_{EE} > 0$ during the contact interval

Table 2. Kinetic energy decomposition T_c and T_a, and parameter ξ

Case	T_c^- (mJ)	T_a^- (mJ)	T_c^+ (mJ)	T_a^+ (mJ)	ξ
1	9.30	$4.4{\cdot}10^{-3}$	$3.2{\cdot}10^{-3}$	$2{\cdot}10^{-3}$	1.00
2	9.26	3.28	$4.9{\cdot}10^{-3}$	2.81	0.75
3	9.34	$6.7{\cdot}10^{-4}$	$4.7{\cdot}10^{-3}$	$2.4{\cdot}10^{-4}$	1.00
4	9.10	3.12	$1.6{\cdot}10^{-3}$	2.85	0.74
5	9.33	0.144	$6.6{\cdot}10^{-3}$	0.130	0.98
6	9.30	4.54	$2.9{\cdot}10^{-3}$	4.06	0.66

Table 3. Measured impulses $\bar{\lambda}$ and $\bar{\beta}$

Case	$\bar{\lambda}$ (N·ms)	$\bar{\beta}$ (N·ms)
1	114.74	0.81
2	113.60	-3.65
3	116.09	0.63
4	114.02	-3.26
5	121.38	0.53
6	119.28	-3.94

and therefore tangential force is opposed to that velocity. This force may have various sources, e.g., friction or even tangential stiffness. However, the normal impulse $\bar{\lambda}$ does not change significantly from one case to the other.

Based on Eqs. (12) and (13), it can be seen that the constraint impulse is fully projected to the SCM, whereas the non-ideal impulsive force can couple the dynamics of both subspaces (SCM and SAM). The effect of non-ideal impulses depends on the projections $\mathbf{P}_c^T\mathbf{B}^T$ and $\mathbf{P}_a^T\mathbf{B}^T$, which depend on the configuration of the multibody system at topology change.

We analyzed three different configurations depending on parameter d. For the first configuration ($d = 0$ m, cases 1-2) the generalized non-ideal impulse $\bar{\mathbf{f}}_N = \mathbf{B}^T\bar{\beta}$ is fully projected to the SAM because $\mathbf{P}_c^T\mathbf{B}^T = \mathbf{0}_{2\times 2}$ and $\mathbf{P}_a^T\mathbf{B}^T = \mathbf{B}^T = [-0.1027 \;\; -0.1235]^T$ m. Note that for both cases (1 and 2) the left-hand side of Eq. (12) is nominally the same,[1] and thus the expected value of $\bar{\lambda}$ should also be the same. There is a small difference between the impulse $\bar{\lambda}$ measured for cases 1 and 2 owing to experimental uncertainty in measurements.

As for the second configuration ($d = 0.1$ m, cases 3-4), the generalized tangential impulse is projected to the SCM and the SAM. For those cases, the aforementioned projections are

$$\mathbf{P}_c^T\mathbf{B}^T = \begin{bmatrix} -0.0027 \\ 0.0009 \end{bmatrix} \text{m} \quad \text{and} \quad \mathbf{P}_a^T\mathbf{B}^T = \begin{bmatrix} -0.0646 \\ -0.1392 \end{bmatrix} \text{m} \tag{19}$$

Then, it can be seen that the value of $\bar{\beta}$ is projected to both the dynamic equations associated with the SCM, Eq. (12), and the equations associated with the SAM, Eq. (13). The same happens for the last configuration ($d = 0.2$ m, cases 5-6). In such a case

$$\mathbf{P}_c^T\mathbf{B}^T = \begin{bmatrix} -0.0192 \\ -0.0027 \end{bmatrix} \text{m} \quad \text{and} \quad \mathbf{P}_a^T\mathbf{B}^T = \begin{bmatrix} -0.0510 \\ -0.1209 \end{bmatrix} \text{m} \tag{20}$$

[1] This is because the configuration is the same in both cases and T_c^- is kept constant.

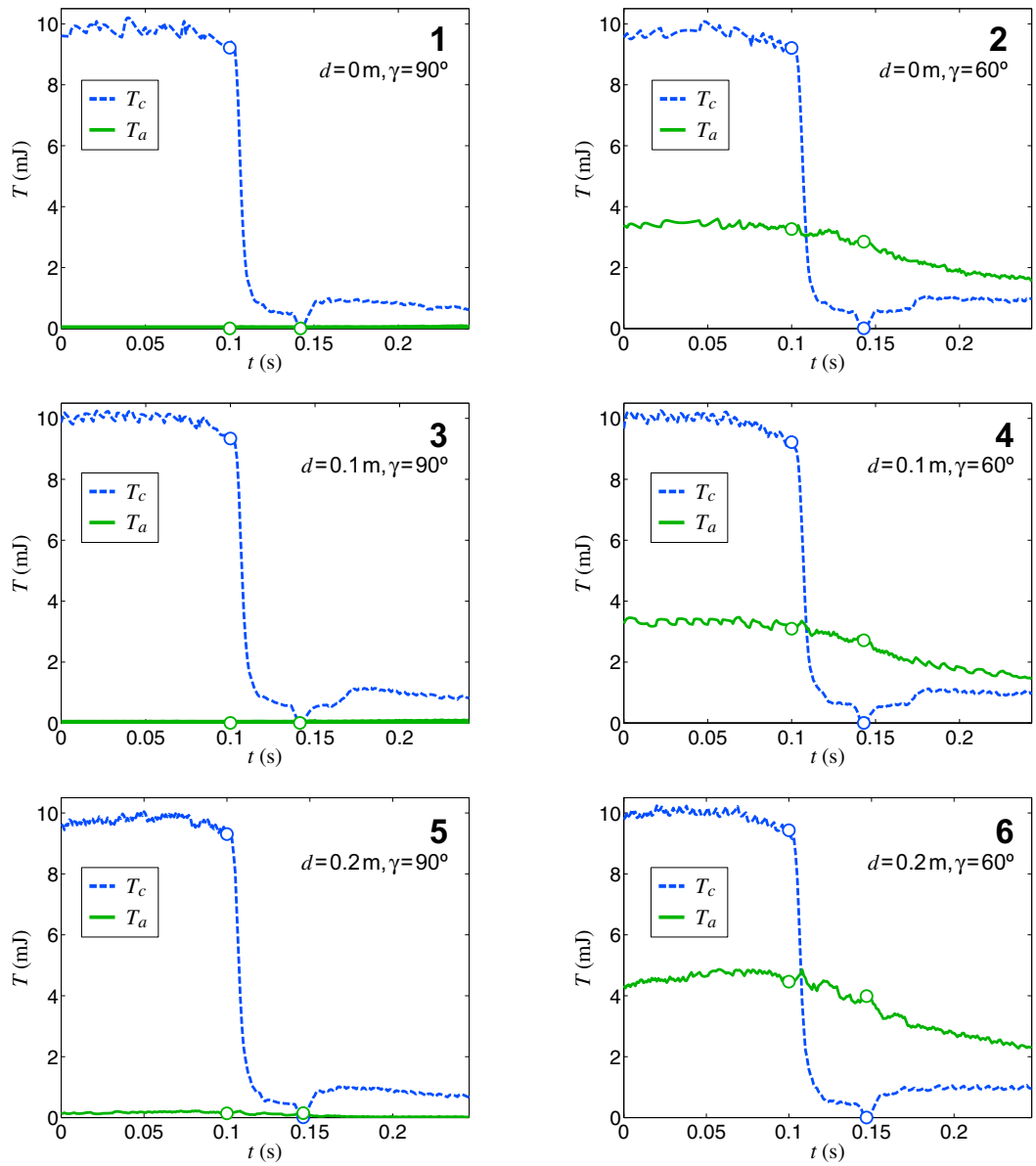

Figure 4. Kinetic energy decomposition T_c, T_a during one individual impact

Note that the term $\mathbf{P}_c^T\mathbf{B}^T$ increases in "magnitude" when parameter d increases. That is, the contribution of the impulse of non-ideal forces on the equation governing the dynamics of the SCM is more significant if the configuration of the mechanism at topology transition is more asymmetric. In cases 5 and 6, the left-hand side of Eq. (12) is nominally the same. The fact that non-ideal impulse $\bar{\beta}$ does have an influence on the SCM dynamics may explain the difference between the measurement of the normal impulse in both cases. This can be observed based on the results shown in Table 3.

Based on Eq. (13) it can be seen that the change in $\mathbf{v}_a$ –and therefore in T_a– is only affected by non-ideal impulsive forces. Cases 2, 4, and 6 are the ones where the tangential impulses $\bar{\beta}$ are higher (see Table 3). This is because for these cases the velocity of the end effector at the pre-event time does have tangential component and forces along that direction are present. These impulses cause changes in $\mathbf{v}_a$ and, at the same time, make the kinetic energy content of the SAM change between t_i^- and t_i^+. This can be observed from the plots shown in Fig. 4 (for individual impacts), and from the averaged results presented in

Table 2. Note that in all these cases (2, 4, and 6), $T_a^+ < T_a^-$, i.e., the kinetic energy of the SAM decreases owing to the tangential contact impulses developed during topology transition.

CONCLUSIONS

In this paper we developed a method for the analysis of topology transitions that can be modeled by means of bilateral impulsive constraints. The Jacobian of such constraints was used to define subspaces of the tangent space of the system, namely the "space of constrained motion" and the "space of admissible motion".

A decoupling of the impulsive dynamic equations characterizing the event of topology change and the kinetic energy of the system was obtained. This provides useful insight for the analysis of kinetic energy redistribution when constraints are suddenly imposed. We paid particular attention on the projection of non-ideal impulses to the aforementioned subspaces, and showed that such impulses may couple the dynamics in these spaces. It was also shown that the influence of non-ideal impulses on the dynamics associated with the space of constrained motion varies depending on the system configuration at topology change.

The presented concepts were experimentally analyzed using an instrumented robotic multibody system undergoing impact with different configurations and velocities. Detailed experimental results and discussions are presented to support and validate the concepts introduced. In this paper we considered the case of having independent constraints. Nevertheless, there may be practical situations where the constraints generated can depend on each other (redundant constraints). This issue will be further addressed in upcoming future publications.

ACKNOWLEDGMENT

This work has been supported by the Natural Sciences and Engineering Research Council of Canada, the Canada Foundation for Innovation, and a Postdoctoral Scholarship from the Technical University of Catalonia (UPC). The support is gratefully acknowledged.

REFERENCES

[1] Hwang, K.H., and Shabana, A.A., 1995, "Effect of Mass Capture on the Propagation of Transverse Waves in Rotating Beams," *J. Sound and Vibration*, **186**(3), pp. 495-525.

[2] Heppler, G.R., and Shabana, A.A., 1993, "On the Dynamic Mass Capture by Flexible Robots," *Control of Flexible Structures* (Morris, A.K., Ed.), pp. 495-525, American Mathematical Society, Providence, RI, USA.

[3] Collins, S.H., Ruina, A., Tedrake, R., and Wisse, M., 2005, "Efficient Bipedal Robots Based on Passive-Dynamic Walkers," *Science*, **307**, pp. 1082-1085.

[4] McGeer, T., 1990, "Passive Dynamic Walking," *Int. J. Robotics Research*, **9**(2), pp. 62-82.

[5] Kuo, A.D., 2002, "Energetics of Actively Powered Locomotion Using the Simplest Walking Model," *ASME J. Biomechanical Engineering*, **124**, pp. 113-120.

[6] Pars, L.A., 1965, *A Treatise on Analytical Dynamics*, Heinemann, London, England.

[7] Pfeiffer, F., 1984, "Mechanische Systeme mit Unstetigen Übergängen," *Ingenieur Archiv*, **54**, pp. 232-240.

[8] Kövecses, J., and Cleghorn, W.L., 2003, "Finite and Impulsive Motion of Constrained Mechanical Systems via Jourdain's Principle: Discrete and Hybrid Parameter Models," *Int. J. Non-Linear Mechanics*, **38**(6), pp. 935-956.

[9] Kövecses, J., 2008, "Dynamics of Mechanical Systems and the Generalized Free-Body Diagram–Part I: General Formulation," *ASME J. Applied Mechanics*, **75**, 061012, pp. 1-12.

[10] Font-Llagunes, J.M., and Kövecses, J., 2009, "Efficient Dynamic Walking: Design Strategies to Reduce Energetic Losses of a Compass Walker at Heel Strike," *Mechanics Based Design of Structures and Machines*, **37**(3).

[11] Blajer, W., 1997, "A Geometric Unification of Constrained System Dynamics," *Multibody System Dynamics*, **7**(1), pp. 3-21.

[12] Kövecses, J., Piedbœuf, J.C., and Lange, C., 2003, "Dynamics Modeling and Simulation of Constrained Robotic Systems," *Trans. Mechatronics*, **8**(2), pp. 165-177.

[13] Modarres Najafabadi, S.A., 2008, *Dynamics Modelling and Analysis of Impact in Multibody Systems*, PhD Thesis, Department of Mechanical Engineering, McGill University, Montreal QC, Canada.

[14] Bahar, L.Y., 1994, "On the Use of Quasi-velocities in Impulsive Motion," *Int. J. Engineering Science*, **32**(11), pp. 1669-1686.

[15] Kövecses, J., and Font-Llagunes, J.M., 2009, "An Eigenvalue Problem for the Analysis of Variable Topology Mechanical Systems," *ASME J. Computational and Nonlinear Dynamics*, **4**(3).